Biomedicine & Pharmacotherapy 196 (2026) 119090

Contents lists available at ScienceDirect

Biomedicine & Pharmacotherapy

journal homepage: www.elsevier.com/locate/biopha

Preclinical evaluation of progesterone combined with EDP-M scheme in 2D and 3D models of adrenocortical carcinoma

Mariangela Tamburello [a,*], Andrea Abate [a], Caterina Boldini [a], Claudia Bonera [a], Gaia Faustini [a], Arianna Bellucci [a], Barbara Buffoli [b], Lorena Giugno [b], Deborah Cosentini [c], Marta Laganà [c], Marika Vezzoli [d], Sara Baldelli [e], Mattia Carini [e], Duilio Brugnoni [e], Guido Alberto Massimo Tiberio [f], Salvatore Grisanti [c], Alfredo Berruti [c], Sandra Sigala [a]

[a] Section of Pharmacology, Department of Molecular and Translational Medicine, University of Brescia, Brescia, Italy
[b] Section of Anatomy and Physiopathology, Department of Clinical and Experimental Sciences, University of Brescia, Brescia, Italy
[c] Oncology Unit, Department of Medical and Surgical Specialties, Radiological Sciences, and Public Health, University of Brescia and ASST Spedali Civili di Brescia, Brescia, Italy
[d] Unit of Biostatistics and Bioinformatics, Department of Molecular and Translational Medicine, University of Brescia, Brescia, Italy
[e] Central Clinical Laboratory, ASST Spedali Civili di Brescia, Brescia, Italy
[f] Surgical Clinic, Department of Clinical and Experimental Sciences, University of Brescia at ASST Spedali Civili di Brescia, Brescia, Italy

ARTICLE INFO

Keywords:
Adrenocortical carcinoma
EDP-M
Progesterone
3D models

ABSTRACT

Background: Adrenocortical carcinoma (ACC) is a rare malignancy with limited therapeutic options. The current standard for advanced disease, the EDP-M regimen (etoposide, doxorubicin, cisplatin, plus mitotane), demonstrates modest efficacy and substantial toxicity, underscoring the need for improved strategies. Previous data from our group suggest that progesterone (Pg) has antitumor activity in ACC. Megestrol acetate, a Pg analog used in supportive oncology, may enhance both efficacy and tolerability of EDP-M. This study investigated the effects of combining Pg with EDP-M in preclinical ACC models (2D and 3D).

Methods: Two ACC cell lines (NCI-H295R, TVBF-7) and three primary cultures (ACC-172, ACC-173, ACC-174) were exposed for 96 h to etoposide, doxorubicin, cisplatin and mitotane to establish IC_{50} values. Pg (7.5–100 μM) was then tested alone or in combination with EDP-M (1/12 ×, 1/6 ×, 1/4 ×, 1/2 × of IC_{50}) in both 2D and 3D cultures. 3D spheroid models were further characterized by Steroidogenic Factor 1 expression and hormone secretion.

Results: EDP-M and Pg each demonstrated concentration-dependent cytotoxicity. Pg at concentrations < 50 μM showed minimal additional benefit to EDP-M, except at higher EDP-M doses (1/2 IC_{50}). By contrast, Pg ≥ 50 μM significantly enhanced EDP-M cytotoxicity across models ($p < 0.001$). In some 3D models, higher EDP-M concentrations (IC_{50} and 2 × IC_{50}) were required to observe a similar effect, emphasizing the translational relevance of 3D models.

Conclusions: Overall, these findings confirm the potential role of Pg in improving EDP-M cytotoxic effects in 2D and 3D ACC models.

1. Introduction

Adrenocortical carcinoma (ACC) is a rare, aggressive malignancy with a high risk of relapse even after radical surgery [1]. The management of metastatic ACC remains particularly challenging [2]. Standard first-line chemotherapy is the EDP-M regimen (etoposide, doxorubicin, cisplatin plus mitotane), introduced in 1992 [3] and subsequently evaluated in an Italian phase II trial [4,5]. This study reported an objective response rate of 48.6 %, including 6.9 % complete remissions, with median progression-free survival of 9.1 months and overall survival of 28.5 months, establishing EDP-M as the most effective systemic therapy for advanced ACC [4,5].

The results of a large, prospective, multicenter, randomized clinical trial (FIRM-ACT trial), which compared the efficacy of EDP-M to that of

* Corresponding author.
E-mail address: mariangela.tamburello@unibs.it (M. Tamburello).

https://doi.org/10.1016/j.biopha.2026.119090
Received 9 December 2025; Received in revised form 13 January 2026; Accepted 3 February 2026
Available online 10 February 2026

streptozotocin and mitotane (Sz-M) as first-line therapy in 304 ACC patients with metastatic, unresectable disease, indicated that EDP-M was the superior regimen [6]. More recently, a study from our referral oncology center in Italy further supported the limited but clinically meaningful efficacy of EDP-M, reporting partial responses in 50 % of patients and median progression-free and overall survival of 10.1 and 18.7 months, respectively [7]. However, as previously mentioned, the efficacy of EDP-M remains limited, since most patients eventually develop resistance, and the prognosis of those with advanced or metastatic disease continues to be poor, with a 5-year overall survival rate below 15 % [1]. To date, novel approaches, including molecularly targeted agents and immune checkpoint inhibitors, have not produced consistent benefits in ACC and remain far less effective than in other tumor types where such therapies have become standard [8]. This underscores the urgent need to optimize the use of EDP-M while awaiting more effective therapeutic strategies.

Pg has been shown to exert antitumor activity across several cancer types [9–12]. Preclinical studies from our group extended this evidence to ACC, providing a rationale for its potential clinical application [13–15]. We demonstrated that Pg induces concentration-dependent, apoptosis-mediated cytotoxicity in vitro, suppresses tumor growth in xenograft models, and reduces the metastatic potential in zebrafish embryos, effects largely mediated through interaction with intracellular Pg receptors (PgRs) [13–15]. Progestins, synthetic analogues of Pg, are widely used in clinical practice. Their primary applications include hormonal contraception [16] and hormone replacement therapy [17]. In oncology, progestins such as megestrol acetate (MA) and medroxyprogesterone acetate have demonstrated antitumor activity, mainly through anti-estrogenic and direct cytotoxic effects, and are approved for the treatment of advanced breast and endometrial cancers [18–21]. Beyond its antitumor activity, MA has been widely used to counteract anorexia/cachexia in cancer patients, with systematic reviews confirming improvements in appetite and weight gain [22].

In our retrospective analysis, the combination of EDP-M and MA (EDP-MM) was tolerated even in ACC patients with poor performance status (PS), potentially enabling administration of EDP-M at doses comparable to those used in patients with better PS. Treatment with MA was overall moderately tolerated: 54.2 % of patients receiving EDP-MM developed progestin-related toxicities, and 16.7 % discontinued due to adverse events. The clinical benefit rate was higher in the EDP-MM cohort (75.0 %) compared with EDP-M alone (60.4 %), while progression-free and overall survival outcomes were comparable between groups [23].

Collectively, preclinical and clinical findings provided the rationale for the phase II PESETA trial, a randomized, double-blind, placebo-controlled study evaluating EDP-M versus EDP-M plus MA in patients with unresectable locally advanced or metastatic ACC (NCT05913427).

As a parallel translational approach to the ongoing phase II PESETA clinical trial, this preclinical study aimed to investigate the antitumor effects of Pg in combination with EDP-M in 2D and 3D models of ACC, including established cell lines and patient-derived primary cultures.

2. Materials and methods

2.1. ACC cell lines

The human NCI-H295R cell line, derived from a primitive ACC in a female patient [24], was obtained from the American Type Culture Collection (ATCC) and cultured as indicated by ATCC. Additionally, the new ACC cell line TVBF-7 [25] was established from a primary culture derived from a perirenal lymph-node metastasis of a male ACC patient who underwent progression after EDP-M. A detailed description of these cell lines can be found in Sigala et al. [26]. All cell lines were periodically tested for mycoplasma and authenticated by genetic profiling using polymorphic short tandem repeat (STR) loci.

2.2. Patient-derived primary culture

Primary ACC cultures (ACC-172, ACC-173, and ACC-174) were established from tumor tissues of patients undergoing surgery at ASST Spedali Civili di Brescia (Brescia, Italy). ACC-172 was derived from the primary mass of a metastatic, cortisol- and androgen-secreting ACC in a female patient progressing after EDP-M; ACC-173 from a local relapse in a male patient treated with mitotane; and ACC-174 from a female patient with peritoneal recurrence after EDP-M (first line) and immunotherapy (second line). Sample collection was approved by the Ethics Committee (NP1924), and informed consent was obtained.

Tumor specimens were enzymatically dissociated, and primary ACC cells were isolated using the Tumor Cell Isolation Kit (Miltenyi Biotec) according to the manufacturer's protocol. Non-tumor cells were magnetically labeled with MACS™ microbead-conjugated antibodies and removed via MACS column separation. Tumor and non-tumor fractions were collected separately, washed in PBS, and cultured in Advanced DMEM/F12 (Thermo Fisher Scientific) supplemented with 10 % FBS (Thermo Fisher Scientific), 292 μg/mL L-glutamine (Merck Italia, Rome, Italy), and 100 IU/mL penicillin + 100 μg/mL streptomycin (Merck Italia). For ACC-173, culture plates were pretreated with poly-L-lysine (0.01 %, Merck Italia) to enhance adhesion. Adrenal origin of the tumor fraction was confirmed by qRT-PCR analysis of Steroidogenic Factor 1 (SF1) gene expression.

2.3. 3D cell cultures

To better mimic the tumor architecture and study the impact of treatment in a more complex preclinical model, 3D tumor models were developed. To define the optimal conditions for spheroid formation (cell density and methylcellulose concentration), preliminary tests were performed.

Spheroids from NCI-H295R and TVBF-7 cell lines and the primary culture ACC-174 were obtained by seeding 10.000 cells per well in 96-well, U-bottom, ultra-low attachment plates (Corning). Spheroids were cultured in standard medium supplemented with 10 % methylcellulose (Merck, Milan, Italy) for 10 days. 3D models were characterized for SF1 expression as well as Ki67 to confirm active proliferation using immunofluorescence.

2.4. Single treatment in 2D cultures

To evaluate the in vitro effects and determine the IC_{50} of the individual components of the standard EDP-M regimen, preliminary experiments were performed to define the optimal range of drug concentrations to be used for each cell line. Then, NCI-H295R, TVBF-7, and primary ACC cultures (ACC-172, ACC-173, and ACC-174) were seeded in flat-bottom 96-well plates at 15.000 cells per well. After 24 h, cells were treated for 96 h with increasing concentrations of etoposide (0.015–100 μM for NCI-H295R, 1–200 μM for TVBF-7, 10–200 μM for primary cultures), doxorubicin (0.05–20 μM for NCI-H295R, 0.1–10 μM for TVBF-7, 1–60 μM for primary cultures), cisplatin (0.5–30 μM for NCI-H295R, 0.05–6 μM for TVBF-7, 1–50 μM for primary cultures), and mitotane (1.5–48 μM for NCI-H295R, 1.5–60 μM for TVBF-7, 15–100 μM for primary cultures). Etoposide and mitotane were obtained from MedChem Express, while cisplatin and doxorubicin were purchased from SelleckChem (DBA Italia, Milan, Italy). At the end of the treatment period, cell viability was assessed using the CellTiter-Glo® Cell Viability Assay (Promega), following the manufacturer's protocol. Luminescence was measured using the EnSight™ Multimode Plate Reader (PerkinElmer).

2.5. Combined treatments in 2D and 3D cultures

To evaluate the combination's effects of Pg and EDP-M, cells were treated with increasing concentrations of Pg (7.5–100 μM) alone or in

combination with various concentrations of EDP-M. The EDP-M regimen was prepared using the IC_{50} values of the individual drugs, specific to each culture, and subsequently diluted to achieve the desired final concentrations. In 2D cultures, each Pg concentration was combined with EDP-M at 1/12 × , 1/6 × , 1/4 × , and 1/2 × IC_{50}. Seeding procedures, treatment time and cell viability assessment were identical to those used for single-drug treatments.

In 3D cultures, the NCI-H295R and TVBF-7 spheroids were treated with EDP-M at 1/2 × , 1 × , and 2 × IC_{50}, while ACC-174 spheroids were treated at 1/12 × , 1/6 × , 1/4 × , 1/2 × , 1 × , and 2 × IC_{50}. In all cases, the spheroids were exposed to single or combined treatments for 96 h.

Spheroid viability was assessed using the CellTiter-Glo® 3D Cell Viability Assay (Promega), according to the manufacturer's instructions. Prior to viability measurements, representative images of selected spheroids were acquired using an Olympus IX51 optical microscope (Olympus, Segrate, Italy) equipped with a 10 × objective to visually assess spheroid morphology.

All treatments involving Pg were performed in culture medium supplemented with Nu-Serum or FBS pretreated with charcoal-dextran to remove endogenous steroid hormones. Hormone-depleted serum was prepared by incubating 2 % charcoal (20 g/L) for 24 h at 4 °C. Charcoal-dextran was purchased from Sigma-Aldrich (Milan, Italy), and Pg from Merck (Milan, Italy).

Drug–drug interactions between Pg and EDP-M were evaluated using both the Highest Single Agent (HSA) model and the combined Bliss–Loewe reference model implemented in "SynergyFinder Plus" web-based tool. The HSA model was selected to assess whether the drug combination exceeded the efficacy of the most active single agent, while the Bliss–Loewe model was applied to account for potential partial overlap or independence in the mechanisms of action of Pg and EDP-M. Synergy scores were calculated across the entire dose matrix and visualized through tri-dimensional synergy plots (heatmaps). Positive scores indicate synergistic interactions (red), values close to zero indicate additive effects (white), and negative scores indicate antagonism (green).

2.6. Immunofluorescence

Cells were cultured on 12 mm poly-L-lysine-coated coverslips, then fixed, permeabilized, and blocked. After overnight incubation at 4 °C with primary antibodies against SF1 (rabbit, 1:100), Ki-67 (rabbit, 1:400), PgR (rabbit, 1:500) (Cell Signaling Technology, Danvers, MA, USA), and Progesterone Receptor Membrane Component 1 (PGRMC1) (mouse, 1:100) (Santa Cruz Biotechnology, Heidelberg, Germany) cells were washed and incubated with Alexa Fluor 488-conjugated anti-rabbit (1:100), Alexa Fluor 488-conjugated anti-mouse (1:100) and Alexa Fluor 594-conjugated anti-rabbit (1:100) secondary antibodies for 1 h at room temperature. Nuclei were stained with Hoechst 33258 (Merck Italia), and F-actin was labeled with Alexa Fluor Plus 647 Phalloidin (Invitrogen). Coverslips were mounted using FluorPreserve™ Reagent (Merck Italia), and fluorescence was visualized with a Zeiss LSM 900 confocal microscope using a 40x/1.30 immersion objective. Image analysis was performed with Zen Blue software 3.8 (Carl Zeiss S.p.A., Oberkochen, Germany).

Spheroids were cultured in 96-well round-bottom plates for 10 days, then collected into 1.5 mL tubes, washed with PBS, and fixed overnight at 4 °C in 4 % (w/v) paraformaldehyde (Immunofix, Bio-Optica, Milan, Italy) under slow rotation. Subsequently, they were permeabilized with 20 % methanol and 0.1 % Triton X-100 in PBS for 15 min. Non-specific binding was blocked by incubation in PBS containing 0.1 % Triton X-100 and 0.2 % BSA for 2 h. Spheroids were incubated with primary antibodies against SF1 (rabbit, 1:100) and Ki-67 (rabbit, 1:400) (Cell Signaling Technology, Danvers, MA, USA) for 24 h at 4 °C. After extensive washing, Alexa Fluor 488-conjugated anti-rabbit (1:100) and Alexa Fluor 594-conjugated anti-rabbit (1:100) secondary antibodies (Jackson ImmunoResearch, West Grove, PA, USA) were applied overnight at 4 °C, together with Hoechst 33258 nuclear counterstaining (Merck Italia). Spheroids were then rinsed in PBS, incubated in 47 % 2,2′-thiodiethanol for at least 24 h at 4 °C, embedded in low-melting agarose, and imaged using a Zeiss LSM 900 confocal laser-scanning microscope equipped with an EC Plan-Neofluar 40 × /1.30 immersion objective (Carl Zeiss S.p.A., Oberkochen, Germany). Zen blue software 3.8 (Carl Zeiss S.p.A.) was used for image analysis and processing.

2.7. Collection of conditioned supernatants

To investigate basal steroid hormone secretion in 2D models, cells were seeded in 6-well plates at a density of 1.5 × 10^6 cells per well. The following day, the culture medium was replaced with serum-free simplified medium (1 mL per 10^6 cells), consisting of a 1:1 (v/v) mixture of DMEM-Low Glucose (Sigma Aldrich) and Nutrient Mixture F-12 Ham (Sigma Aldrich), supplemented with 292 μg/mL L-glutamine (Sigma Aldrich). After 24 h, the medium was collected and stored at –80 °C. For 3D models, spheroids were seeded in 96-well plates at 1 × 10^5 cells per well and cultured for up to 10 days. Approximately 10 spheroids were then collected into a single well and incubated in 0.1 mL of serum-free medium per well for 24 h. The medium was collected and stored at –80 °C.

2.8. Liquid chromatography tandem mass spectrometry (LC–MS/MS) steroid measurements

The collected supernatants were analysed by LC–MS/MS to quantify the secreted steroids. The extraction, chromatographic separation, and quantification in mass spectrometry were performed using the MassChrom® Steroids in Serum/Plasma kit (ChromSystems, Gräfelfing, Germany) following the manufacturer instructions.

2.9. Statistical analysis

All statistical analyses were performed using R (version 4.5.0) and GraphPad Prism software version 10 (GraphPad Software, La Jolla, CA, USA). Data were first checked for completeness, and experimental replicates containing missing values were excluded. For each experimental condition, quantitative variables were summarized as mean ± standard deviation (SD) or, where appropriate, as mean ± standard error of the mean (SEM). When multiple treatments were compared, the data were first checked for completeness and homogeneity of variance.

For global comparison among multiple treatments, a one-way analysis of variance (ANOVA) model was applied, considering treatment as the main factor. When ANOVA indicated significant differences (p-value < 0.05), Tukey's honestly significant difference (HSD) post-hoc test was performed to identify pairwise differences between treatment groups while adjusting for multiple comparisons. For pairwise comparisons between two conditions, the unpaired two-tailed Student's *t*-test was used.

Graphical visualization of the data included bar plots showing mean ± SD, as well as box-and-whisker plots showing the distribution of responses across treatments, and dose-response curves generated by nonlinear regression analysis where data are reported as mean ± SEM. Post-hoc significance levels were highlighted on graphs using standard asterisk notation (p-value < 0.05; p-value < 0.01 (*); p-value < 0.001 (***)).

All statistical tests were two-sided. Each data point represents the mean of at least three independent biological replicates, each performed in technical triplicate. This design ensured adequate statistical power and reproducibility of the observed effects.

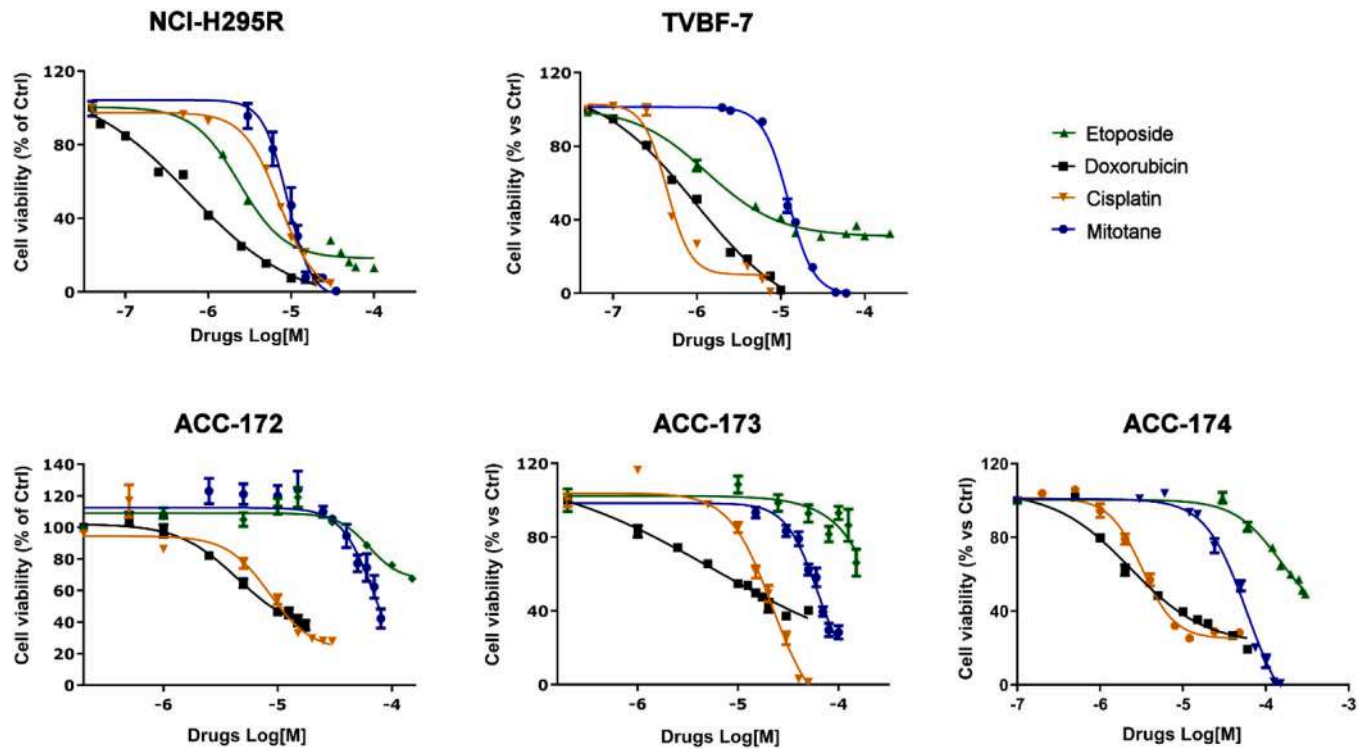

Fig. 1. Effect of etoposide, doxorubicin, cisplatin and mitotane on NCI-H295R and TVBF-7 ACC cell lines and ACC-172, ACC-173 and ACC-174 primary cultures. Cell viability assay was assessed after treatment with increasing concentrations of each drug for 96 h, as described in Methods. Results are expressed as the percentage of viable cells vs. untreated cells. Data are reported as the mean ± SEM of three experiments performed in biological triplicate, with each biological replicate conducted in technical quadruplicate. Concentration-response curves were fitted using a nonlinear regression model (log/inhibitor/ vs. response – variable slope), and IC_{50} values were calculated accordingly.

Table 1
IC_{50} values of EDP-M scheme drugs in ACC cell models.

	Etoposide	Doxorubicin	Cisplatin	Mitotane
NCI-H295R	**2.4 μM** 95 % CI: 2.1–2.6 μM	**0.7 μM** 95 % CI: 0.5 – 1.5 μM	**7.2 μM** 95 % CI: 6.8 – 7.7 μM	**8.9 μM** 95 % CI: 7.4 – 10.9 μM
TVBF-7	**1.3 μM** 95 % CI: 1–1.7 μM	**1 μM** 95 % CI: 0.8 – 1.2 μM	**0.44 μM** 95 % CI: 0.40 – 0.48 μM	**12.2 μM** 95 % CI: 11.7 – 12.9 μM
ACC-172	**62.6 μM** 95 % CI: 42.3 – 91.4 μM	**4.5 μM** 95 % CI: 3.5 – 6.7 μM	**8.4 μM** 95 % CI: 6.8 – 10.4 μM	–
ACC-173	–	**5.9 μM** 95 % CI: 1.3 – 17.4 μM	**21.8 μM** 95 % CI: 16.5 – 28.9 μM	**61.4 μM** 95 % CI: 44.7 – 84.3 μM
ACC-174	–	**2.3 μM** 95 % CI: 1.8 – 2.9 μM	**3.2 μM** 95 % CI: 2.8 – 3.6 μM	**59.8 μM** 95 % CI: 47.8 – 74.8 μM

3. Results

3.1. Effect of etoposide, doxorubicin, cisplatin and mitotane on ACC cell lines and primary cultures

Since the EDP-M regimen is the standard first-line chemotherapy for patients with ACC, we assessed the effect of its individual components (etoposide, doxorubicin, cisplatin, and mitotane) on established ACC cell lines (NCI-H295R and TVBF-7) as well as on primary cultures (ACC-172, ACC-173, and ACC-174). Cells were exposed to increasing concentrations of each drug, and cell viability was measured after treatment. All compounds induced a significant reduction in viability in a concentration-dependent manner across the experimental models tested (Fig. 1). Viability was expressed relative to untreated control cells. Concentration–response curves were generated using GraphPad software, which allowed calculation of half-maximal inhibitory concentrations (IC_{50}) together with 95 % confidence intervals (CI) for each drug and cellular model, summarized in Table 1. As shown in Table 1, IC_{50} values could not be determined for etoposide in ACC-173 and ACC-174 cells, nor for mitotane in ACC-172 cells, as these drugs displayed limited efficacy even at the highest concentrations tested.

3.2. Effects of Pg alone and in combination with EDP-M in ACC cell lines and primary cultures

To further explore the potential role of Pg in ACC, we evaluated its cytotoxic effect both as a single agent and in combination with the EDP-M regimen at sub-IC_{50} concentrations. The IC_{50} values reported above (Table 1) were used to prepare the EDP-M solutions for the combination experiments. When IC_{50} values could not be determined (etoposide in ACC-173 and ACC-174; mitotane in ACC-172), we applied reference IC_{50} values derived from the other primary cultures, corresponding to 62.6 μM for etoposide and 60 μM for mitotane (this value was selected as it approximates the mean of the IC_{50} obtained for the other two ACC primary cultures). NCI-H295R and TVBF-7 cell lines, together with the primary cultures ACC-172, ACC-173, and ACC-174, were then treated

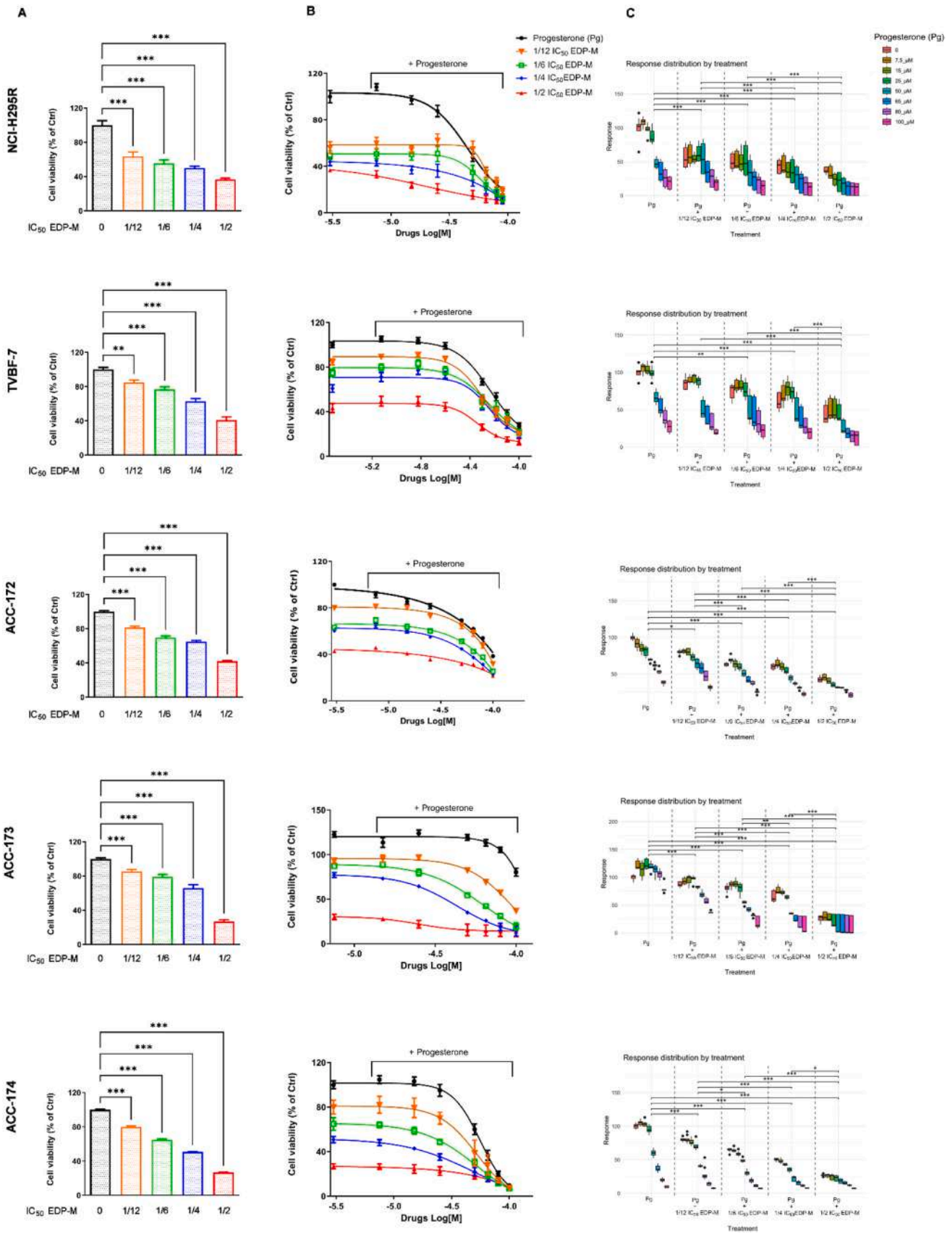

(caption on next page)

Fig. 2. (A) Bar graphs showing cell viability (% of control) after treatment with EDP-M at different fractions of IC_{50} (1/12, 1/6, 1/4, 1/2) in NCI-H295R, TVBF-7, and primary ACC cultures (ACC-172, ACC-173, ACC-174). Data are presented as mean ± SD; p-value < 0.01 (*), p-value < 0.001 (**) p-value < 0.0001 (***), compared with untreated controls. (B) Concentration–response curves for Pg alone and in combination with EDP-M at sub-IC_{50} concentrations. Plots report mean ± SEM of three experiments performed in biological triplicate, with each biological replicate conducted in technical quadruplicate. (C) Viability values are expressed as percentages relative to untreated controls. Each box represents the interquartile range (IQR), while the horizontal line indicates the median, and whiskers extend to 1.5 × IQR from the lower and upper quartiles. The combined treatments produced a concentration-dependent decrease in viability, with a significant potentiation of EDP-M cytotoxicity observed at Pg concentrations ≥ 50 μM. The strongest synergistic effects were detected when Pg ≥ 50 μM was combined with 1/2 IC_{50} EDP-M. Statistical significance versus single-agent treatments was determined by one-way ANOVA followed by Tukey's multiple-comparison test (p-value < 0.05; p-value < 0.01 (*); p-value < 0.001 (**); p-value < 0.0001 (***)).

with increasing concentrations of Pg (7.5–100 μM) and/or EDP-M at 1/12 × , 1/6 × , 1/4 × , and 1/2 × IC_{50}.

As shown in Fig. 2, both EDP-M (A) and Pg (B) exhibited concentration-dependent cytotoxicity when administered as single agents across all models. However, the efficacy and potency of Pg varied among the different ACC cell models, consistent with their distinct Pg receptor expression patterns assessed by immunofluorescence (Supplementary Figure 1). Combinations involving Pg at concentrations below 50 μM did not result in a significant reduction in cell viability compared with EDP-M alone. However, when Pg was applied at concentrations ≥ 50 μM, the combined treatments consistently produced a significantly stronger cytotoxic effect than either agent alone (C).

Importantly, in NCI-H295R and ACC-173 cells, the combination of Pg with EDP-M at 1/2 IC_{50} concentrations produced a significantly greater reduction in cell viability than either Pg or EDP-M alone. To comprehensively assess the interaction between Pg and EDP-M, drug synergy was analysed using both the HSA model and the combined Bliss–Loewe reference model implemented in "SynergyFinder Plus". The HSA model was employed to determine whether the drug combination produced an effect superior to that of either agent alone, whereas the Bliss–Loewe model was used to account for uncertainty regarding the degree of mechanistic overlap or independence between the two compounds.

Bliss–Loewe synergy analysis revealed an intermediate interaction profile, characterized by localized regions of synergy at higher concentrations and antagonistic effects at moderate concentrations across all analysed cell models (Supplementary Figure 7A). Notably, HSA synergy analysis demonstrated that the combination of Pg and EDP-M exhibited synergistic effects in all cell models, with positive synergy scores observed in NCI-H295R (7.58), TVBF-7 (4.45), ACC-172 (8.72), ACC-173 (14.32), and ACC-174 (9.91) cells (Supplementary Figure 7B).

3.3. Characterization of 3D ACC models by SF-1 expression, steroidogenic activity, and proliferation

To evaluate the suitability of 3D culture systems for modelling ACC, we examined SF1 expression, steroidogenic activity, and proliferative status in spheroids derived from the NCI-H295R and TVBF-7 cell lines, as well as from patient-derived ACC-174 cell culture.

Steroidogenic factor-1 (SF-1), a diagnostic biomarker of ACC [27], was assessed by immunofluorescence after 10 days of culture. All three 3D models (NCI-H295R, TVBF-7, and ACC-174) exhibited SF-1 expression at levels comparable to their respective 2D cultures (Supplementary Figure 2), confirming preservation of lineage-specific molecular identity under 3D conditions (Fig. 3).

To assess steroidogenic function, we measured the basal secretion of adrenal hormones. Approximately 60 % of ACC tumors produce adrenal hormones, with cortisol being the most commonly secreted hormone, occurring in 30–40 % of functional ACCs [28].

Thus, basal secretion of 11-deoxycortisol, cortisol, and cortisone was quantified to assess functional steroidogenesis. In NCI-H295R cultures, high levels of 11-deoxycortisol were secreted in 2D compared to 3D conditions ($p < 0.0001$), while cortisol and cortisone secretion did not significantly differ between 2D and 3D (Fig. 3A). In TVBF-7 constructs, cortisone secretion was significantly increased in 3D relative to 2D ($p < 0.01$), whereas 11-deoxycortisol and cortisol remained low under both conditions (Fig. 3B). In primary ACC-174 spheroids, all three hormones were detectable but showed no significant differences between 2D and 3D cultures (Fig. 3C). These data demonstrate that 3D ACC models retain basal steroidogenic activity, with line-specific differences in hormone output.

To characterize proliferative dynamics, spheroids were stained for Ki-67 and imaged by z-stack confocal microscopy. As schematically illustrated (Fig. 4A), proliferative cells localized mainly to the spheroid periphery, with reduced proliferation in deeper layers. Consistent with this organization, NCI-H295R spheroids displayed strong Ki-67 positivity in the outer rim at z1 and z2, whereas in the equatorial section (z3), Ki-67 staining was largely confined to the periphery with markedly reduced signal in the inner region (Fig. 4B and Supplementary Figure 3). TVBF-7 constructs showed a similar distribution, with proliferating cells localized to the spheroid edge and a quiescent central zone (Fig. 4C and Supplementary Figure 4). In contrast, ACC-174 spheroids displayed sparse Ki-67 positivity across all layers, indicating lower proliferative capacity relative to established cell lines (Fig. 4D and Supplementary Figure 5). For completeness, Ki-67 staining of the corresponding 2D cultures is shown in Supplementary Figure 6.

Together, these findings demonstrate that 3D ACC cultures preserve key molecular and functional features of ACC, including SF-1 expression, hormone secretion, and spatial tumour architecture, including peripheral proliferation and reduced activity in central zones. Moreover, differences between established cell lines and patient-derived cultures highlight the capacity of 3D systems to capture model-specific tumour behaviour.

3.4. EDP-M and Pg treatments in 3D spheroid models

In addition to 2D cell lines and primary culture models, we also evaluated the effect of Pg and EDP-M, alone and in combination, on cell viability in a 3D model. This approach is useful for better understanding drug efficacy compared to adherent cultures alone, as cell aggregation in spheroids more closely mimics the tumour architecture and cell–cell interactions.

Consistent with 2D results, both Pg and EDP-M induced a concentration-dependent cytotoxic effect across all ACC models. In NCI-H295R (Fig. 5A) and TVBF-7 spheroids (Fig. 6A), however, four-fold higher concentrations of EDP-M (2 × IC_{50}) were required to achieve residual viability comparable to those observed in 2D at the highest dose tested (1/2 × IC_{50}). In contrast, ACC-174 spheroids retained sensitivity to EDP-M, as comparable cytotoxic effects were obtained using the same concentrations effective in 2D (1/12 ×, 1/6 ×, 1/4 ×, and 1/2× IC_{50}; Fig. 7A). At the highest concentrations (IC_{50} and 2× IC_{50}), EDP-M treatment of ACC-174 spheroids resulted in marked cytotoxicity, with residual viabilities of 10 % ± 4.2 % and 2.6 % ± 2.2 %, respectively (Fig. 7A).

Pg treatment at the maximum concentration (100 μM) showed reduced efficacy in 3D compared with 2D in both NCI-H295R (residual viability: 38 % ± 4.2 % vs. 19.22 % ± 8.8 % in 2D) and TVBF-7 spheroids (47.3 % ± 13.7 % vs. 27.4 % ± 7.5 % in 2D), while responses in ACC-174 spheroids were comparable between 3D and 2D models (11.6 % ± 10.6 % vs. 9.5 % ± 1.4 %). In combined treatments, Pg enhanced the cytotoxic effect of EDP-M. The combination of EDP-M + Pg produced a significantly greater reduction in viability compared

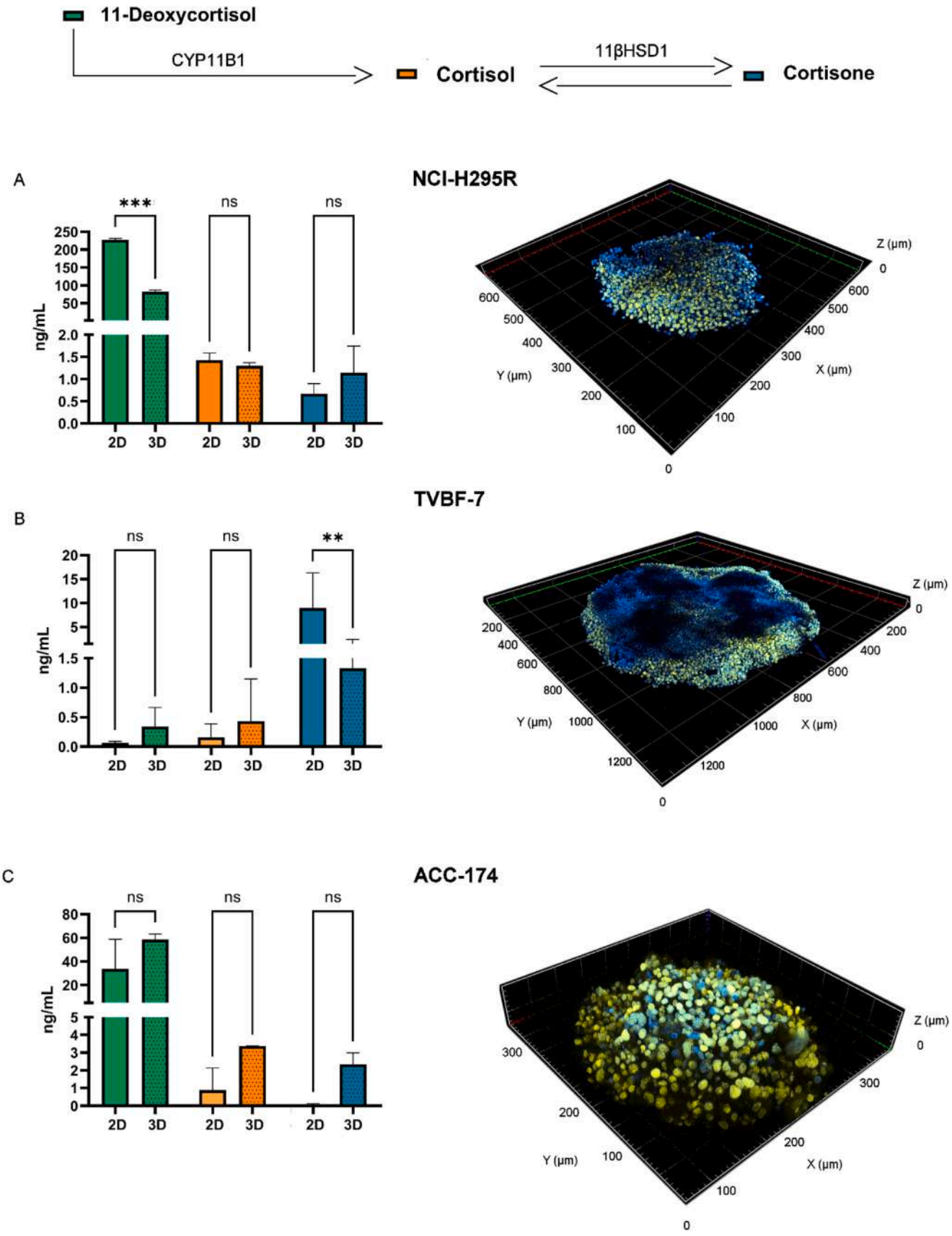

Fig. 3. (A–C) Basal secretion of 11-deoxycortisol (green), cortisol (orange), and cortisone (blue) in 2D versus 3D cultures of (A) NCI-H295R, (B) TVBF-7, and (C) ACC-174 cells. Data are presented as mean ± SD. Statistical comparisons were performed using one-way ANOVA with multiple comparisons (p-value < 0.0001(***), p-value < 0.01(**), ns = not significant). Right panels: representative 3D reconstructions of spheroids after 10 days of culture, showing compact tumor architecture for each cell type and SF-1 staining (yellow).

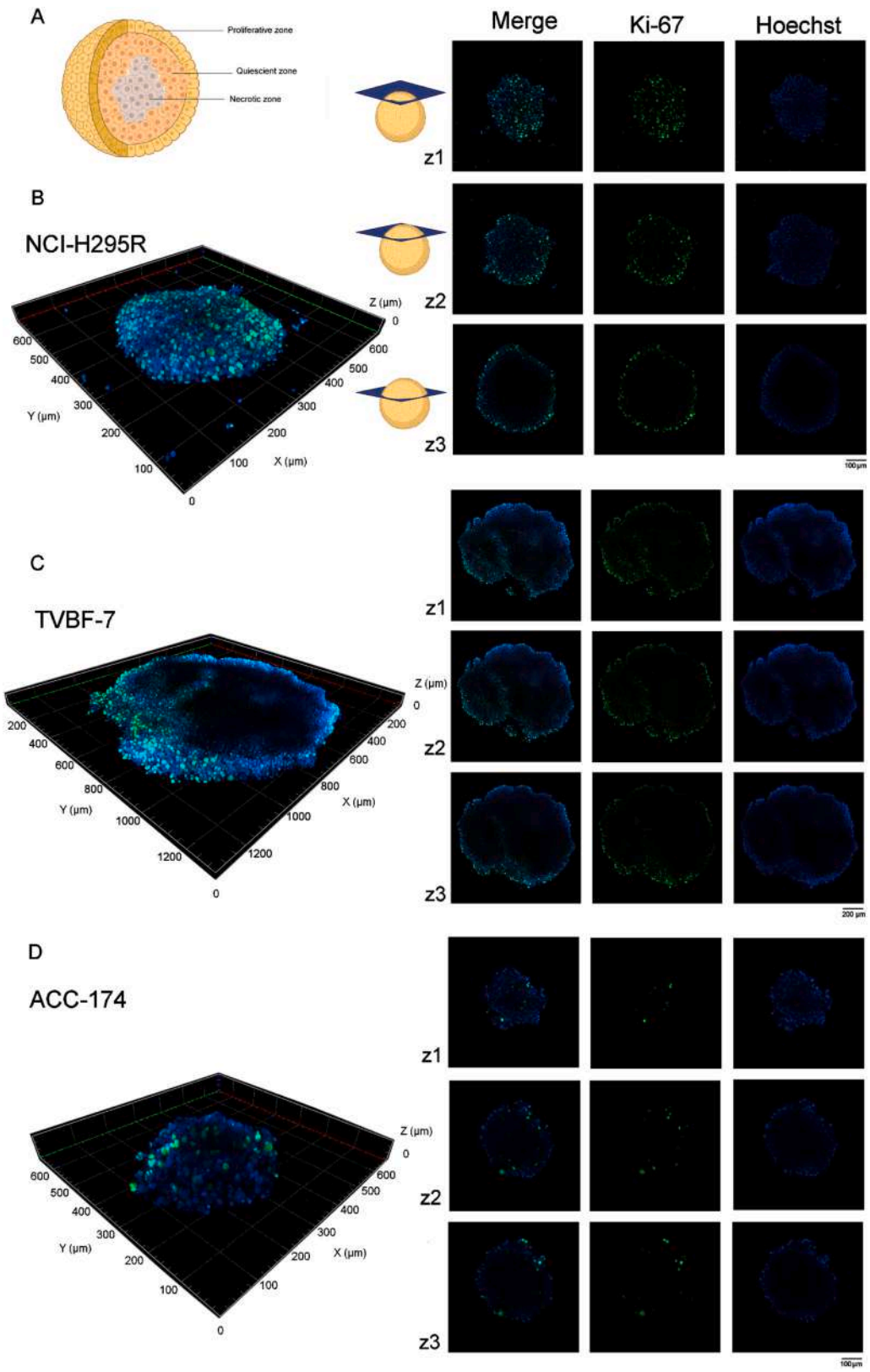

Fig. 4. (A) Schematic representation of proliferative (outer), quiescent (intermediate), and necrotic (core) zones in 3D spheroids. (B–D) Representative 3D reconstructions (left) and z-stack immunofluorescence images (right) of spheroids derived from (B) NCI-H295R, (C) TVBF-7, and (D) ACC-174 cultures after 10 days stained with Ki-67 (green) and Hoechst (blue). z1, z2, and z3 are optical sections at different heights of the spheroid. The smallest section (z1) shows mostly the outer surface, while the largest section (z3, at the equatorial diameter) reveals both the external rim and the inner core. All other confocal optical sections of the spheroid, which were used for 3D reconstruction, are shown as Supplementary Figures.

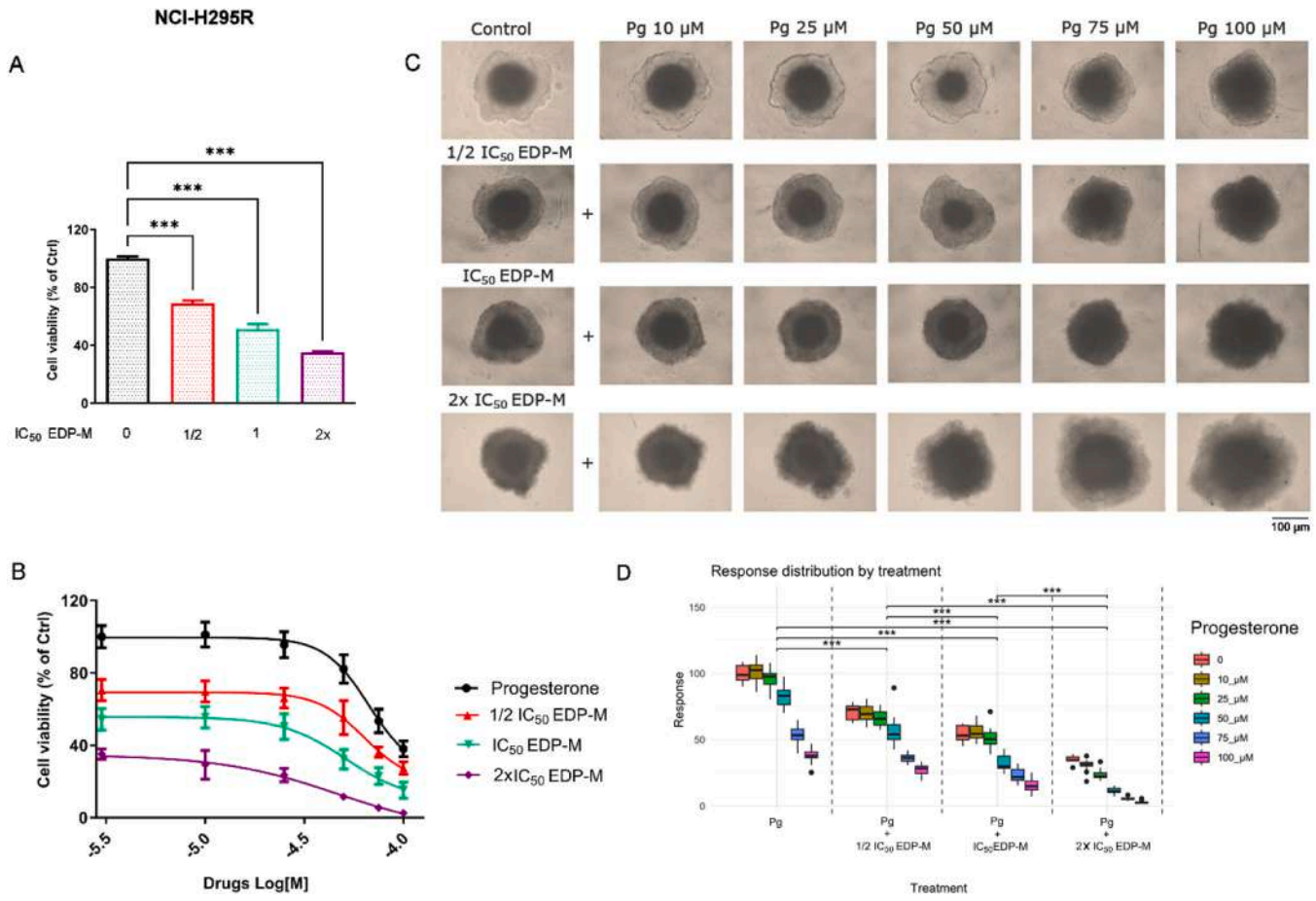

Fig. 5. (A) Bar graphs showing cell viability (% of control) after treatment with EDP-M at different fractions of IC_{50} (1/2, 1 and 2x) in NCI-H295R spheroids. Data are presented as mean ± SD; p-value < 0.0001 (***), compared with untreated controls. (B) Representative images of 3D spheroids treated with EDP-M alone or in combination with Pg (10–100 µM). The images were acquired using an optical microscope equipped with a 10x objective (C) Concentration–response curves for Pg alone and in combination with EDP-M at sub-IC_{50} concentrations. Data are expressed as the mean ± SEM of three experiments performed in biological triplicate, with each biological replicate conducted in technical quadruplicate. (D) Boxplots showing the distribution of viability responses across Pg concentrations and EDP-M doses. Boxes represent the interquartile range (IQR), horizontal lines indicate medians, and whiskers extend to 1.5 × IQR. Combined treatments produced a significant, concentration-dependent reduction in viability compared with single-agent exposures, with maximal cytotoxicity observed for Pg ≥ 50 µM combined with 1/2 × IC_{50} × EDP-M. Statistical significance: p-value < 0.05, p-value < 0.01 (*), p-value < 0.001 (**), p-value < 0.0001 (***).

with EDP-M alone starting at 50 µM Pg ($p < 0.05$). With the highest EDP-M concentration (2 × IC_{50}), the enhanced cytotoxic effect was already evident at the lowest Pg concentrations tested ($p < 0.05$). Synergy analysis was also performed, as previously described, using "SynergyFinder Plus" applying both HAS and Bliss–Loewe models, which yielded concordant results with positive synergy scores in both models, with the exception of TVBF-7 cells under the Bliss–Loewe model. Specifically, Bliss–Loewe synergy scores were 8.78 for NCI-H295R, −1.20 for TVBF-7, and 2.29 for ACC-174, whereas HSA synergy analysis revealed positive synergy across all tested cell models, with scores of 16.17 for NCI-H295R, 11.34 for TVBF-7, and 12.94 for ACC-174 (Supplementary Figures 8). In terms of spheroid morphology, clear differences were observed across all models. Untreated NCI-H295R spheroids displayed a characteristic architecture with a necrotic core and a proliferative outer layer. Following treatment, microscopic inspection confirmed drug-induced damage, as evidenced by diffuse necrosis, progressive loss of spheroid compactness, and irregular margins, likely resulting from cell lysis and release of intracellular contents (Fig. 5C). TVBF-7 spheroids, which typically exhibit a donut-like structure, showed a distinct pattern of necrosis that progressively increased along the edges after treatment (Fig. 6C). In contrast, ACC-174 spheroids responded differently; their size and density were gradually reduced with escalating EDP-M concentrations, and this effect was particularly pronounced when combined with Pg (Fig. 7C).

4. Discussion

The EDP-M regimen represents the current standard first-line systemic therapy for advanced, unresectable adrenocortical carcinoma (ACC), a rare cancer with the 5-year survival rate is less than 15 % among patients with metastatic disease [1].

Although multiple genes and pathways have been identified as potentially targetable in ACC [29], translation of this preclinical knowledge into effective therapies has been disappointing [30–32]. In the absence of effective second-line options, EDP-M will likely remain the standard of care for the coming years, underscoring the importance of strategies aimed at enhancing its efficacy.

In this context, our study focused on evaluating the antitumor activity of Pg in combination with EDP-M using both 2D and 3D models of ACC.

The development of effective therapies critically depends on the availability and adequacy of preclinical models, since the lack of effective targeted therapies largely reflects the limitations of current systems: conventional 2D cultures fail to reproduce the 3D architecture and complexity of human tumours including tissue topography, diffusion kinetics, adhesion peptide availability, and cell–cell interactions, which

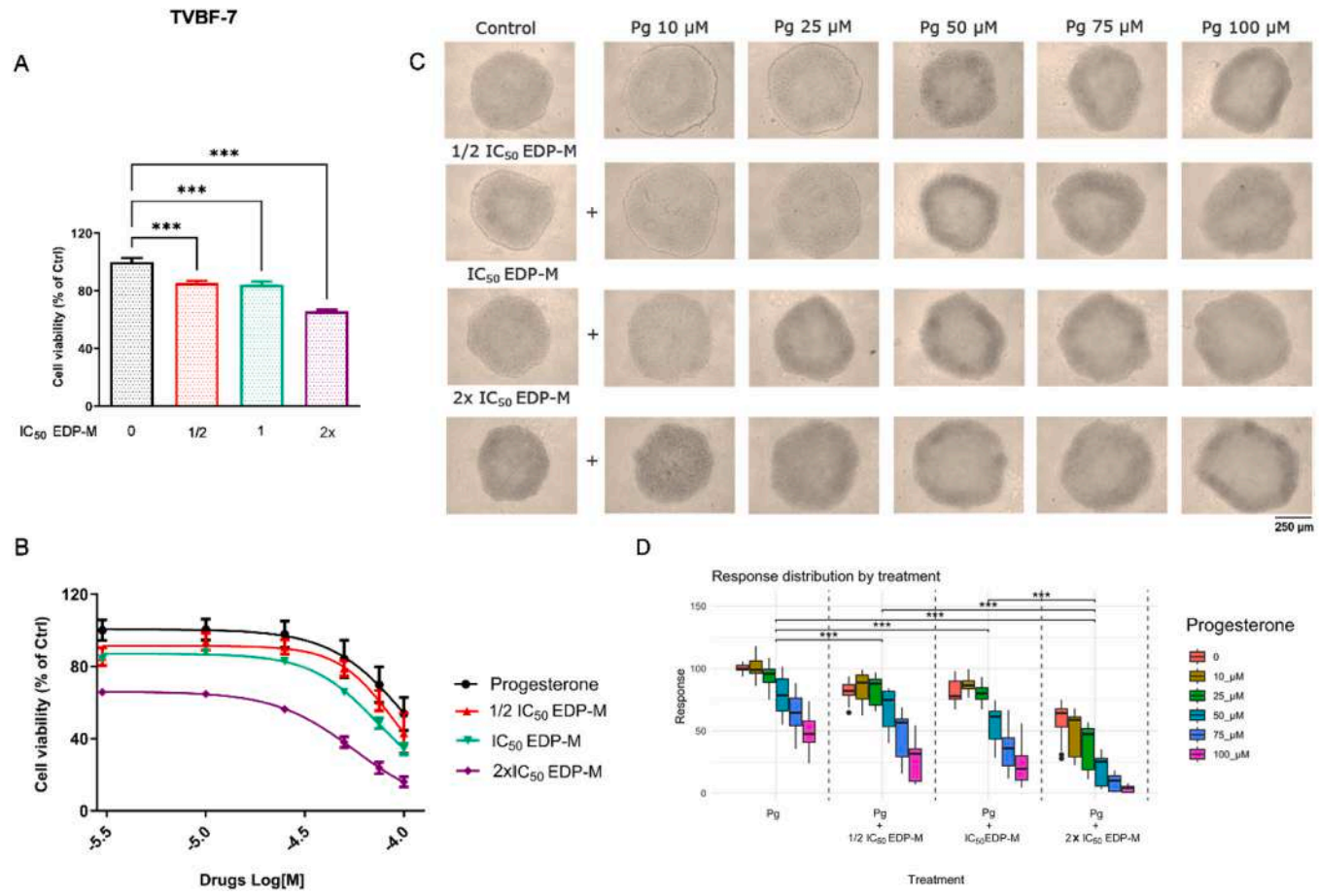

Fig. 6. (A) Bar graphs showing cell viability (% of control) after treatment with EDP-M at different fractions of IC_{50} (1/2, 1 and 2x) in TVBF-7 spheroids. Data are presented as mean ± SD; p-value < 0.0001 (***), compared with untreated controls. (B) Representative images of 3D spheroids treated with EDP-M alone or in combination with Pg (10–100 µM). The images were acquired using an optical microscope equipped with a 10x objective (C) Concentration–response curves for Pg alone and in combination with EDP-M at sub-IC_{50} concentrations. Data are the mean ± SEM of three experiments performed in biological triplicate, with each biological replicate conducted in technical quadruplicate. (D) Boxplots illustrating the distribution of cell-viability responses across Pg concentrations and EDP-M combinations. Boxes represent the interquartile range (IQR), horizontal lines indicate medians, and whiskers extend to 1.5× IQR. Combined treatments produced a significant, concentration-dependent reduction in viability compared with single-agent exposures, confirming a synergistic interaction between Pg and EDP-M. The strongest effect was observed for Pg ≥ 50 µM in combination with 1/2 × IC_{50} EDP-M. Statistical significance: p-value < 0.05, p- value < 0.01 (*), p- value < 0.001 (**), p- value < 0.0001 (***).

can ultimately induce significant genomic and phenotypic alterations [33].

ACC tumours are usually large (>6 cm), necrotic, highly proliferative (Ki67-high), and steroidogenic [34]. Therefore, preclinical models should aim to recapitulate this heterogeneity, including steroid hormone production, variable proliferation, necrosis, and chemotherapy resistance [35]. To overcome these limitations, we sought to establish 3D spheroid models corresponding to each of the 2D cultures used in this study. By generating paired 2D/3D systems, we aimed not only to compare drug responses across culture conditions but also to capture the biological heterogeneity of ACC. Indeed, another key strength of this lies in the diversity of models employed: we studied two established ACC cell lines, one derived from a primary tumour and one from a metastasis, as well as three patient-derived primary cultures with advanced/ metastatic disease, one from a mitotane-treated patient and two from patients previously treated with EDP-M. These cultures directly mirror the clinical context of the ongoing PESETA trial, which is investigating EDP-M with or without MA. This approach, enabled by the integrated strategy of systemic EDP-M followed by resection of residual disease, has become standard practice in Brescia's multidisciplinary management of ACC. Importantly, these patient-derived cultures provide clinically relevant material to study ACC biology and treatment response. By combining established cell lines with primary cultures, our study captures both model reproducibility and the heterogeneity of clinically treated ACC, enhancing the translational relevance of our findings.

The results obtained by treating ACC cell lines (NCI-H295R and TVBF-7) with the individual components of the EDP-M regimen confirmed their cytotoxic efficacy. Drug-induced effects were concentration-dependent, with only minor differences observed in IC_{50} values between the two lines. In contrast, the ACC primary cultures displayed generally higher IC_{50} values, reflecting a more resistant phenotype and further highlighting the intrinsic heterogeneity of ACC pharmacological responses. Notably, the primary cultures were relatively more sensitive to cisplatin and doxorubicin, while showing marked resistance to etoposide and mitotane, so much so that in some cases calculation of an IC_{50} value was not feasible. Overall, efficacy in the primary cultures was limited and detectable only at drug concentrations unlikely clinically achievable.

When the full EDP-M combination was tested, the synergistic activity of its components was confirmed in all treated cell models, demonstrating greater efficacy than single agents.

Exposure of ACC cells to EDP-M in combination with concentrations of Pg higher than 25 µM revealed a clear enhancement of cytotoxicity, independent of the baseline EDP-M drug concentration. NCI-H295R and TVBF-7 cell lines displayed a stronger sensitivity, in line with their higher PgR expression. Conversely, ACC-173 primary cultures were

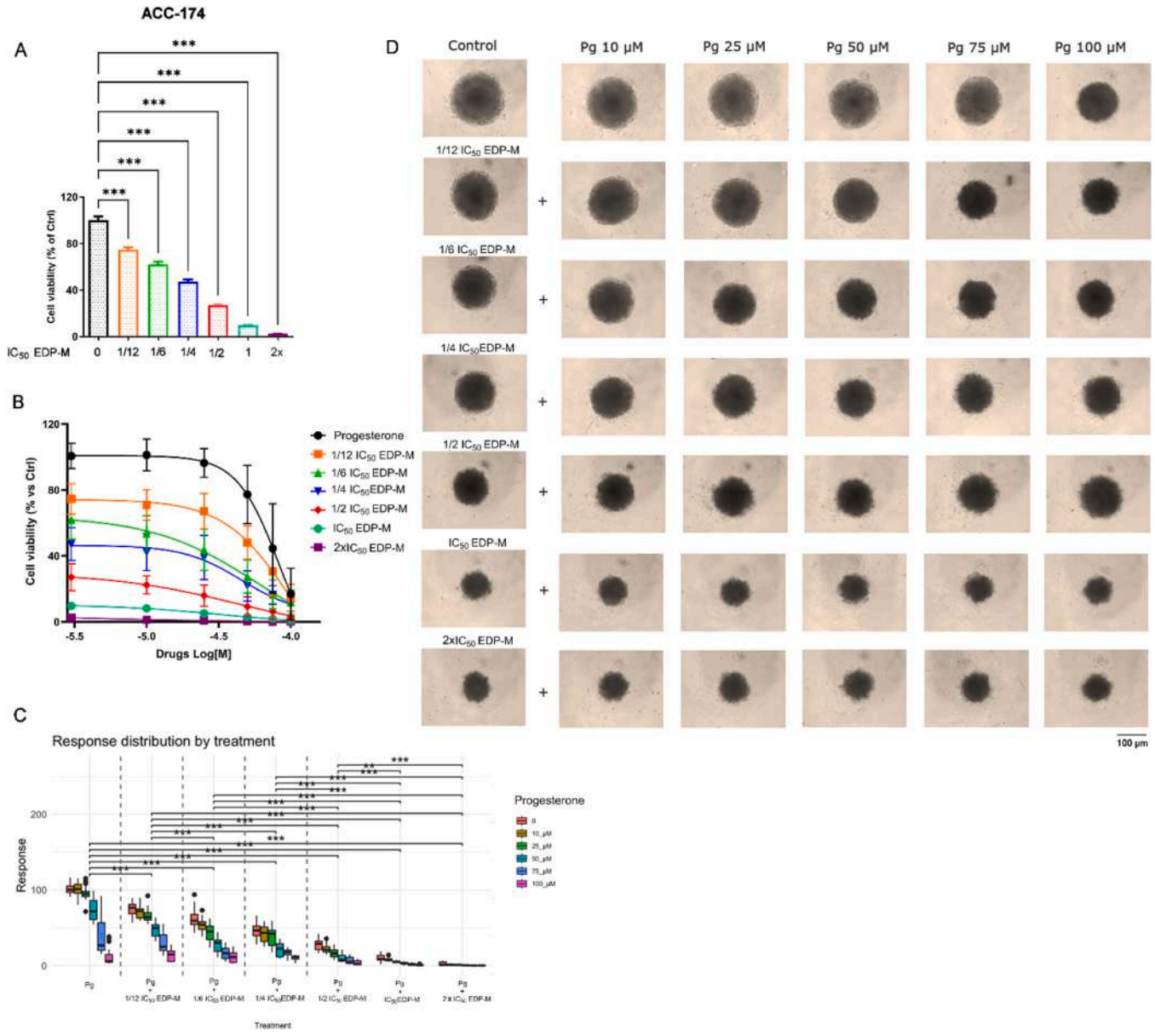

Fig. 7. (A) Bar graphs showing cell viability (% of control) after treatment with EDP-M at different fractions of IC_{50} (1/12, 1/6, 1/4, 1/2, 1 and 2x) in ACC-174 spheroids. Data are presented as mean ± SD; p-value < 0.0001 (***), compared with untreated controls. (B) Concentration–response curves for Pg alone and in combination with EDP-M at sub-IC_{50} concentrations. Data are the mean ± SEM of three experiments performed in biological triplicate, with each biological replicate conducted in technical quadruplicate. (C) Boxplots illustrating the distribution of viability responses across Pg concentrations and EDP-M combinations. Boxes represent the interquartile range (IQR), horizontal lines indicate medians, and whiskers extend to 1.5 × IQR. Combined treatments induced a significant, concentration-dependent reduction in viability compared with Pg or EDP-M alone, confirming a synergistic interaction between the two agents. The strongest cytotoxic effects were observed for Pg ≥ 50 µM in combination with ½× IC_{50} EDP-M, with further reduction at higher EDP-M doses. Statistical significance: p-value < 0.05, p-value < 0.01 (*), p-value < 0.001 (**), p-value < 0.0001 (***). (D) Representative images of 3D spheroids treated with EDP-M alone or in combination with Pg (10–100 µM). The images were acquired using an optical microscope equipped with a 10x objective.

largely resistant to Pg monotherapy, even at high doses, likely reflecting their low PgR expression.

Interestingly, despite its partial resistance to both EDP-M and Pg alone, the ACC-173 primary culture exhibited a marked enhancement of cytotoxicity when exposed to the combination treatment. This observation is consistent with prior findings showing that some PgR-negative ACC primary cultures still reduce viability following Pg exposure, suggesting that PgR expression is not a definitive predictive marker of Pg's antineoplastic activity [14]. Alternative mechanisms may involve membrane-associated progesterone receptors (mPRs), such as Progesterone Receptor Membrane Component 1 (PGRMC1), which mediate so-called "extranuclear" or "non-genomic" Pg effects and may contribute to the observed responses [14,36]. Importantly, the enhanced efficacy of EDP-M combined with Pg observed in 2D cultures was further corroborated in 3D spheroid models, where synergy analyses performed using "SynergyFinder Plus" showed predominantly positive scores across the analysed cell models, indicating a synergistic effect. However, except for ACC174, spheroids were generally more resistant to treatment, requiring higher drug concentrations to achieve comparable cytotoxic effects. In particular, spheroids were largely unresponsive to Pg alone and required EDP-M doses two- to four-fold higher than those effective in 2D cultures to significantly reduce viability. This finding is not unexpected, as previous studies have reported that 3D constructs of ACC are more resistant to mitotane [35] or EDP-M [37], in line with

evidence from other cancer types [38,39].

In our study, all three ACC cell lines continued to proliferate and maintained steroidogenesis in 3D culture for up to 10 days. The presence of confluent necrosis, particularly evident in NCI-H295R spheroids, closely mirrored features of the in vivo tumour architecture. This phenomenon likely results from cellular overcrowding and the consequent competition for nutrients and oxygen within the spheroid core [38], consistent with the hypoxic and nutrient gradients known to drive necrosis in solid tumours [40,41].

In contrast, ACC-174 spheroids show a drug response similar to 2D cultures, likely because seeding the same number of cells produces smaller spheroids than NCI-H295R or TVBF-7, limiting 3D microenvironmental features such as hypoxia-related drug resistance. Indeed, in spheroids, hypoxia develops with size: < 200 μm spheroids are mostly proliferative and normoxic, while ~200–300 μm spheroids show zonation with surface proliferation, central quiescence, and core hypoxia [40,42,43]. The small size of ACC-174 spheroids likely maintains a predominantly proliferative, normoxic state, explaining their 2D-like drug sensitivity.

The differences between 2D and 3D ACC models highlight limitations of monolayer cultures for predicting in vivo responses. While our 3D models lack non-tumor microenvironment cells and anatomical context, they better capture clinically relevant microenvironmental features. The higher EDP-M concentrations required to achieve partial effects in 3D systems emphasize the value of these more complex models in capturing tumour-specific pharmacological responses [37].

In conclusion, our results further support the potential role of Pg in ACC therapy and demonstrate that its combination with EDP-M enhances cytotoxic effects in vitro, reinforcing the value of integrated 2D and 3D preclinical models in guiding future therapeutic strategies. Importantly, as a companion to the ongoing clinical trial, this study provides preclinical insights that can help interpret clinical outcomes and support the rational design of combination therapies aimed at improving efficacy while potentially mitigating toxicity in advanced ACC.

CRediT authorship contribution statement

Andrea Abate: Writing – review & editing, Visualization, Resources, Investigation. **Guido Alberto Massimo Tiberio:** Writing – review & editing, Resources. **Claudia Bonera:** Investigation. **Duilio Brugnoni:** Resources. **Caterina Boldini:** Investigation. **Mattia Carini:** Writing – review & editing, Resources, Investigation. **Lorena Giugno:** Resources, Investigation. **Sandra Sigala:** Writing – review & editing, Supervision, Funding acquisition. **Barbara Buffoli:** Writing – review & editing, Resources, Investigation. **Alfredo Berruti:** Writing – review & editing, Supervision, Funding acquisition. **Arianna Bellucci:** Writing – review & editing. **Salvatore Grisanti:** Writing – review & editing. **Gaia Faustini:** Writing – review & editing, Resources, Investigation. **Sara Baldelli:** Resources, Investigation. **Mariangela Tamburello:** Writing – original draft, Visualization, Validation, Supervision, Software, Resources, Project administration, Methodology, Investigation, Formal analysis, Data curation, Conceptualization. **Marika Vezzoli:** Writing – review & editing, Validation, Software, Investigation, Formal analysis. **Marta Laganà:** Writing – review & editing. **Deborah Cosentini:** Writing – review & editing.

Declaration of Competing Interest

The authors declare the following financial interests/personal relationships which may be considered as potential competing interests: Alfredo Berruti and Sandra Sigala reports financial support was provided by AIRC Foundation for Cancer Research. If there are other authors, they declare that they have no known competing financial interests or personal relationships that could have appeared to influence the work reported in this paper.

Acknowledgements

This research was funded by the AIRC IG23009 project (PI A.B.) and AIRC IG27233 project (PI S.S.), and by University of Brescia local grants. Confocal-based imaging experiments were performed at the Imaging Platform of the Department of Translational and Molecular Medicine of the University of Brescia.

Appendix A. Supporting information

Supplementary data associated with this article can be found in the online version at doi:10.1016/j.biopha.2026.119090.

Data Availability

Data will be made available on request.

References

[1] M. Fassnacht, et al., Adrenocortical carcinomas and malignant phaeochromocytomas: ESMO-EURACAN Clinical Practice Guidelines for diagnosis, treatment and follow-up, Ann. Oncol. 31 (11) (2020) 1476–1490.
[2] F. Megerle, et al., Advanced adrenocortical carcinoma - what to do when first-line therapy fails? Exp. Clin. Endocrinol. Diabetes 127 (2-03) (2019) 109–116.
[3] A. Berruti, et al., Favorable response of metastatic adrenocortical carcinoma to etoposide, adriamycin and cisplatin (EAP) chemotherapy. Report of two cases, Tumori 78 (5) (1992) 345–348.
[4] A. Berruti, et al., Mitotane associated with etoposide, doxorubicin, and cisplatin in the treatment of advanced adrenocortical carcinoma. Italian Group for the Study of Adrenal Cancer, Cancer 83 (10) (1998) 2194–2200.
[5] A. Berruti, et al., Etoposide, doxorubicin and cisplatin plus mitotane in the treatment of advanced adrenocortical carcinoma: a large prospective phase II trial, Endocr. Relat. Cancer 12 (3) (2005) 657–666.
[6] M. Fassnacht, et al., Combination chemotherapy in advanced adrenocortical carcinoma, N. Engl. J. Med 366 (23) (2012) 2189–2197.
[7] M. Laganà, et al., Efficacy of the EDP-M scheme plus adjunctive surgery in the management of patients with advanced adrenocortical carcinoma: the Brescia Experience, Cancers 12 (4) (2020).
[8] V. Cremaschi, et al., Advances in adrenocortical carcinoma pharmacotherapy: what is the current state of the art? Expert Opin. Pharm. 23 (12) (2022) 1413–1424.
[9] X. Kong, et al., Progesterone induces cell apoptosis via the CACNA2D3/Ca2+/p38 MAPK pathway in endometrial cancer, Oncol. Rep. 43 (1) (2020) 121–132.
[10] Y. Liu, et al., Effects of estradiol and progesterone on the growth of HeLa cervical cancer cells, Eur. Rev. Med. Pharm. Sci. 21 (17) (2017) 3959–3965.
[11] H.R. Motamed, et al., The apoptotic effects of progesterone on breast cancer (MCF-7) and human osteosarcoma (MG-636) cells, Physiol. Int 107 (3) (2020) 406–418.
[12] R. Schürmann, M. Cronin, J.U. Meyer, Estrogen plus progestin and colorectal cancer in postmenopausal women, N. Engl. J. Med. 350 (23) (2004) 2417–2419, author reply 2417-9.
[13] C. Fiorentini, et al., Antisecretive and antitumor activity of abiraterone acetate in human adrenocortical cancer: a preclinical study, J. Clin. Endocrinol. Metab. 101 (12) (2016) 4594–4602.
[14] M. Fragni, et al., In vitro antitumor activity of progesterone in human adrenocortical carcinoma, Endocrine 63 (3) (2019) 592–601.
[15] M. Tamburello, et al., Preclinical evidence of progesterone as a new pharmacological strategy in human adrenocortical carcinoma cell lines, Int J. Mol. Sci. 24 (7) (2023).
[16] R. Erkkola, B.M. Landgren, Role of progestins in contraception, Acta Obstet. Gynecol. Scand. 84 (3) (2005) 207–216.
[17] R.A. Lobo, The role of progestins in hormone replacement therapy, Am. J. Obstet. Gynecol. 166 (6 Pt 2) (1992) 1997–2004.
[18] M.A. Altinoz, et al., Medroxyprogesterone and tamoxifen augment anti-proliferative efficacy and reduce mitochondria-toxicity of epirubicin in FM3A tumor cells in vitro, Cell Biol. Int 31 (5) (2007) 473–481.
[19] C.D. Cobau, et al., A randomized trial of megestrol acetate with or without premarin in the treatment of potentially responsive metastatic breast cancer. A Study of the Eastern Cooperative Oncology Group (E2185), Cancer 77 (3) (1996) 483–489.
[20] M. García-Sáenz, et al., Understanding progestins: from basics to clinical applicability, J. Clin. Med. 12 (10) (2023) 3388.
[21] H.B. Muss, et al., Megestrol acetate versus tamoxifen in advanced breast cancer: 5-year analysis–a phase III trial of the Piedmont Oncology Association, J. Clin. Oncol. 6 (7) (1988) 1098–1106.
[22] V. Ruiz Garcia, et al., Megestrol acetate for treatment of anorexia-cachexia syndrome, Cochrane Database Syst. Rev. 2013 (3) (2013) Cd004310.
[23] A. Turla, et al., Feasibility and activity of megestrol acetate in addition to etoposide, doxorubicin, cisplatin, and mitotane as first-line therapy in patients with metastatic/unresectable adrenocortical carcinoma with low performance Status, Cancers 15 (18) (2023).

[24] W.E. Rainey, K. Saner, B.P. Schimmer, Adrenocortical cell lines, Mol. Cell Endocrinol. 228 (1-2) (2004) 23–38.
[25] S. Sigala, et al., A comprehensive investigation of steroidogenic signaling in classical and new experimental cell models of adrenocortical carcinoma, Cells 11 (9) (2022).
[26] S. Sigala, et al., An update on adrenocortical cell lines of human origin, Endocrine (2022).
[27] S. Sbiera, et al., High diagnostic and prognostic value of steroidogenic factor-1 expression in adrenal tumors, J. Clin. Endocrinol. Metab. 95 (10) (2010) E161–E171.
[28] T. Else, et al., Adrenocortical carcinoma, Endocr. Rev. 35 (2014) 282–326.
[29] A.M. Lerario, D.R. Mohan, G.D. Hammer, Update on biology and genomics of adrenocortical carcinomas: rationale for emerging therapies, Endocr. Rev. 43 (6) (2022) 1051–1073.
[30] M. Fassnacht, et al., Linsitinib (OSI-906) versus placebo for patients with locally advanced or metastatic adrenocortical carcinoma: a double-blind, randomised, phase 3 study, Lancet Oncol. 16 (4) (2015) 426–435.
[31] M. Kroiss, et al., Sunitinib inhibits cell proliferation and alters steroidogenesis by down-regulation of HSD3B2 in adrenocortical carcinoma cells, Front Endocrinol. 2 (2011) 27.
[32] M. Laganà, et al., Phase II study of cabazitaxel as second-third line treatment in patients with metastatic adrenocortical carcinoma, ESMO Open 7 (2) (2022) 100422.
[33] A. Skardal, et al., A reductionist metastasis-on-a-chip platform for in vitro tumor progression modeling and drug screening, Biotechnol. Bioeng. 113 (9) (2016) 2020–2032.
[34] a, *Epidemiology, Presentation, Staging, and Prognostic Factors in Adrenocortical Carcinoma*, bookTitle= Primary Adrenal Malignancies, Springer Nature Switzerland, Cham, 2025, pp. 1–6.
[35] S. Feely, et al., Development and characterization of 3-dimensional cell culture models of adrenocortical carcinoma, Endocrinology 166 (1) (2024).
[36] D. Garg, et al., Progesterone-mediated non-classical signaling, Trends Endocrinol. Metab. 28 (9) (2017) 656–668.
[37] P.H. Dedhia, et al., A 3D adrenocortical carcinoma tumor platform for preclinical modeling of drug response and matrix metalloproteinase activity, Sci. Rep. 13 (1) (2023) 15508.
[38] S. Breslin, L. O'Driscoll, The relevance of using 3D cell cultures, in addition to 2D monolayer cultures, when evaluating breast cancer drug sensitivity and resistance, Oncotarget 7 (29) (2016) 45745–45756.
[39] E. Reidy, et al., A 3D view of colorectal cancer models in predicting therapeutic responses and resistance, Cancers 13 (2) (2021).
[40] S. Däster, et al., Induction of hypoxia and necrosis in multicellular tumor spheroids is associated with resistance to chemotherapy treatment, Oncotarget 8 (1) (2017) 1725–1736.
[41] X. Jing, et al., Role of hypoxia in cancer therapy by regulating the tumor microenvironment, Mol. Cancer 18 (1) (2019) 157.
[42] J.P. Freyer, R.M. Sutherland, Regulation of growth saturation and development of necrosis in EMT6/Ro multicellular spheroids by the glucose and oxygen supply, Cancer Res 46 (7) (1986) 3504–3512.
[43] W. Mueller-Klieser, J.P. Freyer, R.M. Sutherland, Influence of glucose and oxygen supply conditions on the oxygenation of multicellular spheroids, Br. J. Cancer 53 (3) (1986) 345–353.